Encapsulation of vitamin D3 using rhamnolipids-based nanostructured lipid carriers

Maria A. Azevedo [a,b], Miguel A. Cerqueira [a,*], Catarina Gonçalves [a], Isabel R. Amado [a], José A. Teixeira [b], Lorenzo Pastrana [a]

[a] International Iberian Nanotechnology Laboratory, Av. Mestre José Veiga, 4715-330 Braga, Portugal
[b] Centre of Biological Engineering, University of Minho, Campus de Gualtar, 4710-057 Braga, Portugal

ARTICLE INFO

ABSTRACT

This work had as main objective to encapsulate vitamin D3 (VD3) into nanostructured lipid carriers (NLCs) using rhamnolipids as surfactant. Glycerol monostearate and medium chain triglycerides with 2.625 % of VD3 were used as lipid materials. The three formulations of NLCs with VD3 (NLCs + VD3) were composed by 99 % of aqueous phase, 1 % of lipid phase and 0.05 % of surfactant. The difference between them was the ratio of solid: liquid in lipid phase. The NLCs + VD3 sizes ranged between 92.1 and 108.1 nm. The most stable formulation maintaining their caracteristics for 60 days at 4 °C. The NLCs + VD3 cytotoxicity demonstrated that concentrations of 0.25 mg/mL or lower up had a good biocompatibility in vitro. During the in vitro digestion, formulations with lower sizes and higher content on solid lipid had higher lipolysis rate and consequently higher VD3 bioaccessibility. The rhamnolipids-based NLCs are a good option for the encapsulation of VD3.

1. Introduction

In many developing countries and some industrialized, vitamin deficit is a serious health problem leading to deficiency syndromes. In this way, some approaches like supplementation or food fortification have been used as solutions to fix this problem. Vitamins are small organic molecules that have an essential role in human body's growth, maintenance, and development. Also, these molecules can prevent diseases and promote a normal operation of the metabolism. However, humans cannot synthetize vitamins, except for D, K and B3, meaning that they must be obtained from food or supplements (Katouzian & Jafari, 2016). Vitamins are classified as water-soluble and liposoluble being the latter poor soluble in aqueous mediums and very sensitive and unstable when exposed to inadequate conditions (e.g., temperature and pH) (Gonnet et al., 2010).

Although humans can synthesize vitamin D, most people lack this vitamin (Marques et al., 2019). The vitamin D is a liposoluble vitamin and humans can get this vitamin essentially through the skin exposure to the sunlight, from some food products (e.g., egg yolks, fish, cod liver oil,

animal's livers and mushrooms) or from dietary supplements (Gupta et al., 2019; Holick, 2007; Marques et al., 2019). Two forms of vitamin D can be found: vitamin D_2 and vitamin D_3 also called ergocalciferol and cholecalciferol, respectively. Vitamin D_2 comes from mushrooms or plants sources being synthesized from ergosterol under exposure to UV irradiation. Vitamin D_3 is produced from 7-dehydrocholesterol in the human or animal skin also through sunlight action (Gupta et al., 2019; Hewison, 2012). Vitamin D_2 and D_3 are not considered equivalent, vitamin D_2 has an extra methyl group which leads to a decrease in its efficiency in conversion to 25(OH)D and lower affinity with vitamin D-binding protein and vitamin D receptor when compared with vitamin D_3 (Gupta et al., 2019). After the synthesis or ingestion of vitamin D, both forms are converted by the liver in 25-hydroxyvitamin D [25(OH)D] being this form the main circulating metabolite of vitamin D and the reference to measure the amount or status of vitamin D in the organism (Holick, 2007). Relatively to the optimal levels of 25-hydroxyvitamin D [25(OH)D] in human body, consequently of vitamin D, there is no consensus. However, in general, a concentration lower than 20 ng/mL (50 nmol/L) in serum is considered vitamin D deficiency (Grant et al.,

2020; Gupta et al., 2019; Hewison, 2012; Holick, 2007; Tipchuwong et al., 2017). Vitamin D plays an important function in calcium and phosphorus absorption and besides that, helps in calcium storage, being these actions essential to maintain a good bones health (Gupta et al., 2019; Holick, 2007; Marques et al., 2019). The lack of this vitamin can cause rickets in children and osteomalacia/osteoporosis in adults due to inadequate/deficiency bone mineralization (Holick, 2007; Pludowski et al., 2018). Moreover, vitamin D deficiency is also associated with other diseases like cardiovascular disorders, infectious and autoimmune diseases and cancers. For example, studies have shown that vitamin D has a solid immunomodulatory capacity which is fundamental to combat or prevent autoimmune diseases and chronic inflammatory states. This vitamin is also related to components in the cardiovascular system. Studies show that vitamin D can be an important factor in reducing the risk of cancers like breast and colorectal or colorectal adenomas (Pludowski et al., 2018). Considering the importance of vitamin D for the human organism, vitamin D deficiency is a global. The lack or deficiency of this vitamin can be related to low sun exposure, physiologic factors like breast-feeding, obesity, pregnancy and aging, climatic conditions, low vitamin D intake and medication. Besides that, vitamin D is easily degraded when exposed to light, air, humidity, heat or inappropriate pH levels, and also exhibits poor water solubility and oral bioavailability (Gupta et al., 2019; Pludowski et al., 2018).

In recent years, researchers understood that the use of nanotechnology, more specifically nanoencapsulation, is a valuable alternative to protect the vitamins' properties and improve their delivery (Gonnet et al., 2010; Katouzian & Jafari, 2016). However, the nanosystem selection and the nanoencapsulation technique to encapsulate essential vitamins are two crtitical steps to maintain the physicochemical characteristics of the vitamins. Some parameters are important to consider before nanoencapsulation, e.g., the nature of the vitamin, the required size, the physicochemical properties and the material used (Katouzian & Jafari, 2016). In the case of liposoluble vitamins like vitamin D that have a hydrophobic nature and issues related to stability, dissolution, absorption and metabolism, it is necessary to use lipid-based nanosystems with surface properties suitable for aqueous environments and a hydrophobic core for the encapsulation. In this way, lipid-based nanosystems like oil-in-water nanoemulsions (NEs), liposomes, solid-lipid nanoparticles (SLNs) and nanostructured-lipid carriers (NLCs) are the nanosystems more appropriate for nanoencapsulation of liposoluble vitamins (Gupta et al., 2019; Tamjidi et al., 2013). The major difference between these lipid-based nanosystems is their matrix which gives them different properties. The NLCs result from some SLNs limitations (e.g., drug escape through the matrix over time and lower drug loading efficiency). To facilitate the incorporation of drugs, a part of solid lipid used in SLNs development was replaced by liquid lipids. Nowadays, due to their biocompatibility and properties, the NLCs have more advantages and potential as carrier of drugs when compared with SLNs (Salvi & Pawar, 2019). In a previous work, NLCs with glycerol monostearate (GM) and medium-chain triglycerides (MCT) using rhamnolipids (biosurfactant) as emulsifier were developed (Azevedo et al., 2021). The results showed the possibility to produce NLCs using rhamnolipids which represent an important step for the development of rhamnolipids-based NLCs and using them as nanocarriers of liposoluble compounds. The nanoencapsulation of vitamin D into NLCs can be a good option to protect its properties and increase the bioavailability. For example, Park et al. (2017) developed NLCs for the encapsulation and controlled release of vitamin D3. They obtained NLCs with a diameter of 132.9 nm and demonstrated that the stability and protection of VD3 during the gastric phase being>90 % of the VD3 released in intestinal phase. However, the NLCs were produced using high-pressure homogenization and Tween 80 (synthetic surfactant) was used as emulsifier (Park et al., 2017). Taking into account the possibility of encapsulating vitamin D using NLCs and the potentiality of the previous work using rhamnolipids as surfactant to develop NLCs, so the present work aims to develop and characterize rhamnolipids-based NLCs loading VD3. In addition, loaded

NLCs were studied *in vitro* regarding their citotoxicity and vitamin D bioaccessibility. The results presented in this work will contribute to the use of biosurfactant-based nanosystems for the delivery of vitamins and a better understanding of the effect of the lipid fraction (solid:lipid ratio) in the bioaccessibility of vitamins.

2. Experimental section

2.1. Materials

Glycerol monostearate (GM), > 95.0 % monoglyceride, was purchased from Alfa Aesar (Thermo Fisher (Kandel) GmbH, Germany). Vitamin D_3 1.0 Mio IU/g in MCT-oil (composed by 80–100 % of medium-chain triglycerides, 2.50——2.75 % of vitamin D_3 (cholecalciferol) and max. 1 % of vitamin E (DL-α-tocopherol) as stabilizer) was kindly donated by BASF (BASF SE, Germany) being during the manuscript referred as MCT + VD3. Rhamnolipids (a mixture of mono- and dirhamnolipids with 35 % − 45 % of monorhamnolipids and produced by *Pseudomonas aeruginosa*) were provided by NatSurFact (NatSurFact Laboratories, USA). The dimethyl sulfoxide (DMSO) (anhydrous, ≥ 99.9 % of purity), hexane anhydrous (95 % of purity), isopropyl alcohol (≥99.9 % of purity), methanol (Honeywell Chromasolv, 99.9 % of purity), ethanol (≥99.8 % of purity), sodium pyruvate solution 100 mM, resazurin sodium salt were obtained from Sigma-Aldrich (Merck Group KGaA, Germany). Minimum essential media (MEM) was purchased from Thermo Fisher Scientific (Thermo Fisher Scientific Inc., United States) and trypsin-EDTA (0.25 % trypsin; 0.1 % EDTA), penicillin/streptomycin 100x, fetal bovine serum (FBS), non-essential aminoacids (NEAA) were bought from Merck Millipore (Merck Group KGaA, Germany). Relatively to the salts used to prepare the stock simulated solutions for *in vitro* digestion, KCl, NaHCO3, NaCl, MgCl2(H2O)6, (NH4)2CO3 and CaCl2(H2O)2 were all purchased from Sigma-Aldrich (Merck Group KGaA, Germany) and KH2PO4 was purchased from PanReac AppliChem (Spain). The enzymes (pepsin in powder form from porcine gastric mucosa and pancreatin from porcine pancreas) and bile bovine in powder used to simulate the digestion were also obtained from Sigma-Aldrich (Merck Group KGaA, Germany).

2.2. General procedures and characterizations

2.2.1. Production of nanostructured lipid carries with VD3 (NLCs + VD3)

The NLCs + VD3 were prepared according to the method reported by Azevedo et al. (2021) with some modifications (Azevedo et al., 2021). In this case, the lipid phase (LP) consisted in MCT + VD3 and GM as liquid lipid (L) and as solid lipid (S), respectively. The MCT used already had between 2.50——2.75 % of VD3, therefore, increasing the amount of liquid lipid (MCT) in the NLC results in higher concentrations of VD3's, with the following order: NLCs1 + VD3 < NLCs2 + VD3 < NLCs3 + VD3. The rhamnolipids used as surfactant (Sf) were dissolved in ultra-pure water and used as the aqueous phase (AP). The aqueous and lipid phases were homogenized and heated at 75 °C in different glass beakers. After that, the AP was mixed with the LP under high shear homogenization using an ultra-turrax (IKA Ultra-Turrax T18 digital with S18-10G dispersing element, IKA®-Werke GmbH & Co. KG, Germany) at 14,200 rpm for 15 min at 75 °C. The mixture (AP + LP) was then sonicated through an ultrasonic processor (Branson Digital Sonifier Model 450, Branson Ultrasonics Corporation, USA) for 20 min (1 s pulse and 1 s off) with 65 % of amplitude at 75 °C. To complete the process, the mixture was put in ice for 20 min. Considering the sensibility of VD3, all the procedure was done protecting the VD3 from light.

2.2.2. NLCs characterization

2.2.2.1. *Size, polydispersity index, zeta potential and turbidity.* The average particle size, polydispersity index (PDI) and zeta potential (ζ) of

NLCs + VD3 were measured using a Dynamic Light Scattering (DLS) apparatus (Dynamic Light Scattering System SZ-100Z, Horiba Instruments Inc., USA). The turbidity allows evaluating the nanoparticle stability in solution and this parameter was measured through the absorbance at 600 nm using NanoDrop spectrophotometer (NanoDrop 3300, Thermo Fisher Scientific, USA).

The size and PDI were measured using polystyrene cuvettes and the zeta potential using a 6 mm electrode carbon cell. For the turbidity, a quartz cuvette with a path length of 10 mm was used. All measurements were performed at 25 °C using fresh samples diluted 10 times and each measurement of size (by intensity) and PDI were measured with a detection angle of 90° being the zeta potential performed with a detection angle of 173°. For all the measurements at least five replicates were performed.

2.2.2.2. Transmission electron microscopy (TEM). TEM micrographs were performed by transmission electron microscopy (TEM) (JEOL JEM 2100 - HT – 80–200 kV LaB6 gun, JEOL Ltd, Japan) being the images digitally recorded using an UltraScan® 4000 CCD camera (Oneview, Gatan, USA). Grids coated with an ultrathin carbon film (400 mesh, approx. grid hole size of 42 μm, PELCO®, TED PELLA INC., USA) were used to deposit the samples and UranyLess EM Stain (Electron Microscopy Sciences (EMS), USA) was used as the contrast agent. After 24 h, the samples were dried and the micrographs were taken.

2.2.2.3. Small-angle X-ray scattering (SAXS). The structural and crystallinity changes over time were characterized by small angle X-ray scattering (SAXS) (SAXSess mc^2 Kratky camera, Anton Paar GmbH, Austria). The measurements were performed using fresh samples of NLCs (in solution) being prepared in sealed capillaries (Hilgenberg, Germany) without any dilution. All the samples were measured using a Cu-Kα radiation ($\lambda = 1.54056$ Å) and were operated at 40 kV, 50 mA and 25 °C. Also, was used an image plate system covering the q-range from 0.23 to 26 nm^{-1} being the exposure time of 60 min for all samples. The SAXS-quant software (Anton Paar GmbH, Austria) was used to convert the 2D scattering images to 1D radial intensity profiles.

2.2.2.4. Stability during storage. To evaluate the stability of NLCs + VD3 in solution, fresh samples were stored at different temperatures (4 °C, 25 °C and 37 °C). For this study, the size, PDI, zeta potential and turbidity were measured, while the morphology and structural changes were determined by TEM and SAXS, respectively.

2.2.3 Cytotoxicity assessment of NLCs + VD3

2.2.3.1. Cell culture. Caco-2 cells were used to assess the cytotoxicity of NLCs + VD3. Caco-2 cells, clone HTB-37, obtained from the American Type Culture Collection (ATCC) were cultured (passage 25 – 40) in culture flasks containing minimum essential medium (MEM), supplemented with 20 % FBS, 1 % of sodium pyruvate, 1 % non-essential amino acids (NEAA) and 1 % penicillin/streptomycin. The cells were kept at 37 °C and 5 % of CO$_2$. The culture media was replaced every 2/3 days and the cells were sub-cultured assuring a maximum confluence of 70——80 %. To detach adherent cells, trypsin-EDTA was used for 5 min.

2.2.3.2. Resazurin assay. The cytotoxicity of samples was indirectly evaluated by the resazurin reduction assay after 24 or 48 h of contact. Empty or loaded NLCs with VD3 were tested at a concentration range between 0.1 and 1.0 mg/mL of NLCs. Caco-2 cells were seeded onto 96-wells plates at a density of 10 000 cells per well and left adhering overnight. After adhesion, the culture medium was removed and replaced by the samples diluted (10 %) in the culture medium. Before the dilution of samples in the culture medium, the samples were filtrated through a Thermo Scientific™ Polyethersulfone (PES) syringe filters 0.2 μm of pore size and 30 mm of diameter. Milli-Q water (10 % v/v) and

DMSO (10 % v/v) in culture medium were used as negative and positive controls, respectively. The cells were incubated for 24 h or 48 h with samples or controls. At the time point, the samples and controls were removed and added resazurin diluted in culture medium. After 3 h of incubation at 37 °C, the cellular metabolic activity was determined by measuring the fluorescence of resofurin ($\lambda_{excitation} = 560$ nm, $\lambda_{emission} = 590$ nm) using a microtiter plate reader (Synergy H1 – BioTek, BioTek Instruments, Inc., United States). The results are expressed as a percentage in relation to the negative control.

2.2.4. In vitro gastrointestinal digestion, lipolysis and bioaccessibility

2.2.4.1. In vitro digestion. In vitro digestion of NLCs + VD3 was performed according to the standardized INFOGEST protocol for static *in vitro* digestion (Brodkorb et al., 2019). Before starting the digestion procedure, the pepsin activity and trypsin activity (in pancreatin) was assessed to calculate the amount (mg/mL) needed of each enzyme in the *in vitro* digestion. Amylase was not used since there was no starch present in the digested sample. The addition of gastric lipase was omitted due to the limited access of the commercially available enzyme. The trypsin activity was assessed through the kinetic spectrophotometric rate determination method (absorbance at 247 nm). The method is based on the hydrolysis of p-toluene-sulfonyl-L-arginine methyl ester (TAME) by trypsin where one unit corresponds to the hydrolysis of 1 μmol of TAME per minute at pH 8.1 and 25 °C. Pepsin activity assay is based on the spectrophotometric stop reaction method. One unit will produce a ΔAbs280 of 0.001 per minute measured at TCA-soluble products (pH 2 and 37 °C). Bile acids concentration was measured following the supplier's protocol which provides a fluorometric method to measure the total bile acids. According to the results obtained, pepsin (13.8 mg/mL), bile salts (80.0 mg/mL) and pancreatic enzymes (148.2 mg/mL) were freshly prepared just before the digestion procedure.

Stock electrolytic solutions, such as simulated salivary fluid (SSF), simulated gastric fluid (SGF) and simulated intestinal fluid (SIF) were prepared 1.25 times concentrated, considering the later dilution (4:1) with enzymes and CaCl$_2$(H$_2$O)$_2$ added just before the assay to avoid precipitation, according to the INFOGEST protocol.(Brodkorb et al., 2019) The digestion process was performed in an Eppendorf ThermoMixer® C (Eppendorf^{TM} ThermoMixer Temperature Control Device, Eppendorf AG, Germany) to keep the temperature at 37 °C and proper mixing (300 rpm). Pre-heated solutions were used throughout the procedure to avoid any temperature fluctuations.

The digestive process was performed as follows: Oral phase – 5 mL of sample were mixed with 4 mL of SSF, 25 μL of CaCl$_2$(H$_2$O)$_2$ and 975 μL of Milli-Q water, being incubated while mixing for 2 min at 37 °C. Gastric phase - To the oral phase solution was added 8 mL of SGF with 1 mL of pepsin and 5 μL of CaCl$_2$(H$_2$O)$_2$. Then the pH was adjusted to 3.0 using HCl 3.0 mol/L (varying between 19 and 21 μL, depending on the sample). Besides that Milli-Q water was added in order to achieve the 20 mL and it was incubated and mixed during 2 h at 37 °C. Intestinal phase - The gastric phase solution was mixed with 7.7 mL of SIF, 3.3 mL of bile salts, 5 μL of CaCl$_2$(H$_2$O)$_2$ and 5 mL of pancreatic enzymes. After that NaOH 1.0 M was added (varying between 100 or 140 μL, depending on the sample) to adjust pH to 7.0. At the end, the volume was made up to 40 mL with Milli-Q water. This phase was maintained during 2 h under mixing and temperature at 37 °C.

2.2.4.2. Lipolysis – pH-stat method. The lipid hydrolysis was evaluated during the intestinal phase measuring the NaOH (0.05 N) added (titration) to maintain the pH at 7.0. This assessment was based on the release of free fatty acids (FFAs) and leading to the need of NaOH addition to neutralize the FFAs generated and keep pH at 7.0. Until the gastric phase, the process was performed as described before. Then, the 20 mL of gastric phase were transferred into a 120 mL beaker and placed into a water bath at 37 °C with magnetic stirring. Afterward, 7.7 mL of SIF, 3.3

mL of bile salts and 5 μL of $CaCl_2(H_2O)_2$ were added and pH was adjusted to 6.95 ($\pm$0.05) using HCl 3 M or NaOH 1 M. Lastly, the volume was made up to 35 mL with Milli-Q water and 5 mL of pancreatic enzymes were added. Once the pancreatic enzymes were added, the volume of 0.05 N NaOH solution required to keep the pH at 7.0 was recorded for 2 h using a pH-stat device (907 Titrando, Metrohm AG, Switzerland). After the 2 h incubation, the pH was increased to pH 9 and maintained for 30 min being the volume of 0.05 N NaOH added also recorded. Based in the works of Tan, Li, et al. (2020) and Tan, Zhang, et al. (2020), the second step is necessary because at pH 7.0 not all of FFAs generated during lipid digestion are fully deprotonated (Tan, Li, Liu, Muriel Mundo, et al., 2020; Tan, Zhang, Muriel Mundo, et al., 2020). This way, increasing the pH until 9.0 allows to stop the reaction and neutralize and detect any fatty acids that were not ionized under neutral conditions. The total volume of NaOH dispensed in these two steps was used to calculate the total amount of FFAs released Eq. (1).(Li & McClements, 2010)

$$FFAs\,(\%) = \frac{V_{NaOH} \times m_{NaOH} \times M_{lipid}}{W_{lipid} \times 2} \times 100 \qquad (1)$$

Where, V_{NaOH} is the volume of NaOH added to neutralize the FFAs generated (L), m_{NaOH} is the molarity of the NaOH solution (mol/L), M_{lipid} the molecular weight of lipids (g/mol) and W_{ipid} is the weight of lipids (g). The molecular weights of lipids used were calculated taking into account the ratio of each lipid component in the lipid phase being 500.00 g/mol and 358.56 g/mol for MCT + VD3 oil and GM, respectively. Blank experiments were performed: (1) using Milli-Q water instead of sample and (2) SIF instead of pancreatin to evaluate the presence of FFAs in the simulant fluids or in sample that might have contributed to the measured volume but do not result from digestion. The volume of NaOH required to titrate the blank samples were subtracted to the volume of NaOH required to titrate the samples.

2.2.4.3. Extraction of VD3 and its quantification by high performance liquid chromatography (HPLC).

METHOD 1: The VD3 extraction using dimethyl sulfoxide (DMSO) and quantification by HPLC was based on the method used by Maurya & Aggarwal (2019) with slight modifications. For the extraction of VD3, 0.5 mL of sample was taken and put in a flask with 1 mL of DMSO. The mixture was incubated at 45 °C in an Eppendorf ThermoMixer® C (Eppendorf™ ThermoMixer Temperature Control Device, Eppendorf AG, Germany) for 30 min followed by cooling at room temperature. Then, 2 mL of hexane were added to the mixture and vortexed for 1 min, allowing to stand for at least 10 min without agitation until the observation of a phase separation. The upper layer (hexane with free VD3) was removed and collected to a new flask, repeating the extraction three times with the same volume of hexane. After pooling together the three organic phases ($\approx$ 6 mL), the solvent was evaporated at 45 °C for 40 min using a modular centrifugal evaporator (Thermo Scientific™ Digital Series SpeedVac™ Systems - SPD121P, Thermo Fisher Scientific Inc., United Sates). Samples ($\approx$ 0.5 mL) were filtered through 0.2 μm Hydrophobic Fluoropore™ (PTFE) syringe filters (Merck Millipore Ltd, Ireland) to amber HPLC vials. The VD3 was quantified by HPLC (UHPLC - Agilent 1290 - Infinity II LC System, Agilent, United Sates) equipped with a Kinetex® C18 column (150 $\times$ 4.6 mm with particle size 2.6 μm and pore size 100 Å). The HPLC was operated in isocratic mode using 95 % hexane and 5 % isopropyl alcohol as mobile phase with a flow rate of 0.6 mL/minute. The VD3 detection was done at a wavelength of 265 nm using a DAD detector. The column temperature and injection volume were 25 °C and 10 μL, respectively.

Quantification was achieved using the comparison between observed peak areas in the samples and in the calibration curve (VD3 concentrations between 0.001 and 0.135 mg/mL dissolved in hexane). Chromatographic conditions were the same for standard solutions and samples.

METHOD 2: The extraction of VD3 from initial NLCs and digested samples was also performed following the methods of Schoener, et al. (2019) and Tan et al. (2019), with slight modifications (Schoener et al., 2019; Tan et al., 2019). To extract VD3, 0.5 mL of sample were mixed with 1 mL of hexane:ethanol (1:1, v/v). The mixture was vortexed and then centrifuged (Universal 320, Hettich ZENTRIFUGEN, Germany) at 1789 g for 2 min. After centrifugation, the supernatant was collected and put in a new flask, repeating the process two more times. After that, the supernatants from the 3 consecutive extractions were mixed and dried using a modular centrifugal evaporator (Thermo Scientific™ Digital Series SpeedVac™ Systems - SPD121P, Thermo Fisher Scientific Inc., United States) at 50 °C during 40 min. Following sample evaporation, 0.5 mL of methanol were added to redissolve the VD3 that was filtered through 0.2 μm Hydrophobic Fluoropore™ (PTFE) syringe filters (Merck Millipore Ltd, Ireland) for HPLC analysis. The HPLC analysis was done using the same equipment and procedure used in method 1.

A calibration curve was also done using methanol to quantify VD3 in the samples. The concentration's range was 0.008–0.396 mg/mL. The chromatographic conditions were the same for standard solutions and samples.

2.2.4.4. Bioaccessibility of VD3.

Before the extraction and quantification of VD3, the intestinal samples were centrifuged (Universal 320, Hettich ZENTRIFUGEN, Germany) at 4000 g for 30 min at room temperature. The centrifugation led to the separation mixed micelles and solid phase being the micelle phase where VD3 is dispersed. The bioaccessibility of encapsulated VD3 after digestion was calculated using the following equation (Afonso et al., 2020):

$$Bioaccessibility\,(\%) = \frac{m_{micelle}}{m_{initial}} \times 100 \qquad (2)$$

Being $m_{micelle}$ the mass of VD3 in the micelle fraction after digestion and $m_{initial}$ the initial mass of encapsulated VD3.

The measurements of VD3 concentrations in the micelle phases were determined by HPLC using the Mtd1 as extraction method. This method showed to be more efficient and adequate which can be explained by the presence of the digestion fluids, salts and enzymes used that lead to the degradation of NLCs and consequent extraction of VD3.

2.2.4.5. Confocal microscopy.

The structure of the NLCs + VD3 before and after gastric and intestinal phases was studied using a confocal scanning laser microscope (Confocal microscope LSM 780, Zeiss, Germany) to capture the images. The samples were stained with Nile Red (9-diethylamino-5H-benzo[α]phenoxazine-5-one, 0.1 g/L in PEG 200, 2:1 (dye:sample) v/v) making the oil droplets visible. The samples were placed in a glass microscope slide and covering with glass cover slip and was excited with a 488 nm argon laser line.

2.3. Statistical analysis

Statistical analyses were performed using Microsoft Excel 2003 and GraphPad Prism (Version 5.00 (Trial), edition 2007, GraphPad Software, Inc., La Jolla, CA, USA). All the experiments subjected to statistical analyses were carried out at least in duplicate. The statistical analyses were performed using analysis of variance (ANOVA) followed by Tukey's multiple-comparison test ($\alpha = 0.05$) to assess the statistical significance of differences between groups of data. Differences in experimental results were considered statistically significant at 95% confidence level ($p < 0.05$).

3. Results and discussions

3.1. Morphologic properties of NLCs + VD3

Three formulations of NLCs were used for encapsulation of VD3. All the formulations had in common the ratio of AP:LP (%) and the

surfactant percentage, being 99:1 and 0.05, respectively. The difference between them was the ratio of S:L (%) wich was 20:80 for NLCs1 + VD3, 15:85 for NLCs2 + VD3 and 10:90 for NLCs3 + VD3.

Results showed differences in the obtained sizes related to the S:L ratio used, reaching values of 92.07 ± 3.16 nm, 98.89 ± 2.37 nm and 108.1 ± 1.94 nm for NLCs1 + VD3, NLCs2 + VD3 and NLCs3 + VD3, respectively. The sizes increased significantly ($p < 0.05$) when the liquid lipid and consequently the concentration of VD3 increased. The main reasons for the size increase can be the disorder and less dense structure of NLCs with a higher amount of liquid lipid (i.e., a higher amount of solid lipid results in a crystalline and ordered structure). The higher liquid lipid concentration can also be responsible for the increase of interfacial tension or swelling of the core of NLCs and, as a consequence, to increase their size (Soleimanian et al., 2018). Relatively to the PDI, the obtained values ranged between 0.217 and 0.258 and the formulations were not statistically different from each other ($p > 0.05$). These PDI values mean that the size distributions of NLCs + VD3 were quite narrow which can favor their long-term stability (Tamjidi et al., 2013; Bezerra et al., 2019). The zeta potential was also measured and the values obtained were $- 80.94 \pm 6.635$ mV, $- 90.97 \pm 6.75$ mV and $- 92.99 \pm 1.48$ mV to NLCs1 + VD3, NLCs2 + VD3 and NLCs3 + VD3, respectively. Considering these high zeta potential values, the NLCs + VD3 can be considered stable (Azevedo et al., 2021). It is expected that the main responsible for the NLCs + VD3 charge are the rhamnolipids used as surfactant. The rhamnolipids have carboxylic acid groups with pKa values around 4—5, and when they are in a water-based systems with pH above 5 the carboxylic acid groups are charged ($–COO^-$) making the rhamnolipids anionic. Through the absorbance at $\lambda = 600$ nm it is possible to assess the turbidity and visual appearance of the NLCs-based solutions. As expected, the turbidity was smaller to NLCs1 + VD3 which present the smallest sizes ($p < 0.05$). Smaller particles scatter less light than the bigger ones being the absorbance values lower for NLCs with smaller sizes (Uluata et al., 2016). The NLCs showed a spherical and uniform shape which did not depend on the ratio of solid:liquid lipid (Fig. 1) being the size in agreement to the values obtained by DLS. Moreover, Soleimanian et al. (2018) mentioned that the spherical form of NLCs can be an evidence of a less ordered crystalline structure of the lipids because an ordered structure leads to elongated crystals (Soleimanian et al., 2018).

3.2. Stability over time

The NLCs1 + VD3, NLCs2 + VD3 and NLCs3 + VD3 were submitted at different storage temperatures (4 °C, 25 °C and 37 °C) and their stability was evaluated over time, by the evaluation of size, PDI, zeta potential, turbidity, morphology, and structural changes.

In general, all NLCs + VD3 maintained their size, PDI, zeta potential, turbidity and structure for longer time when the storage temperature was 4 °C. Therefore, results showed that NLCs3 + VD3 was the formulation more stable, being the next one the NLCs2 + VD3 (Fig. 2a and Table S1 in Supporting Information). This fact confirmed the influence of solid:liquid lipid ratio in the in lipid phase in the stability of NLCs. The NLCs with lower concentrations of solid lipid (GM) were more stable, and GM's crystallization pattern might be the main reason for the instability of the formulations. The polymorphism can increase the flocculation and coalescence due to higher surface and hydrophobic interactions between particles (Babazadeh et al., 2017). The TEM images of NLCs1 + VD3 at 4 °C after 20 days of storage (Fig. 2b) are an example where is possible to see the coalescence phenomenon which occurs over time. Besides that, through the TEM images, it was also observed an increase of heterogeneity that is in agreement with PDI and turbidity values. Fig. 2c shows the SAXS profiles of the NLCs1 + VD3 over time at different temperatures and it is possible to see a peak emerging at q ~ 1.3 nm^{-1} over time. This peak corresponds to real space periodicities of $d = 4.7$ to 4.9 nm being similar with d spacing expected for the β phase of GM. Probability, over time the GM starts slowly
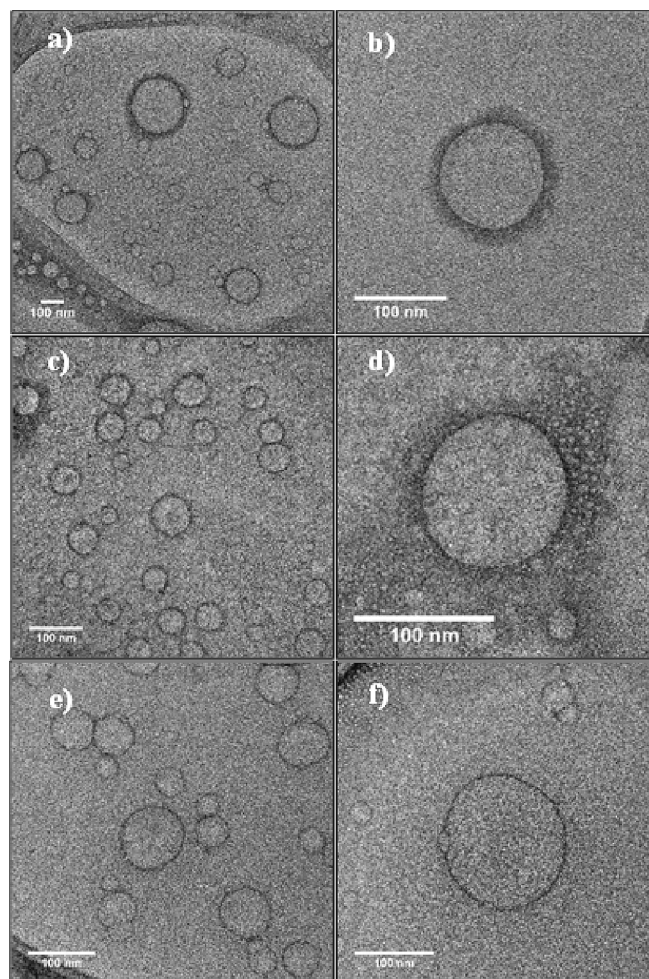
Fig. 1. Transmission electron microscopy (TEM) images of NLCs + VD3: a) and b) NLCs1 + VD3; c) and d) NLCs2 + VD3; e) and f) NLCs3 + VD3. Scale bar: a) 100 nm, 30000x; b) 100 nm, 100000x; c) 100 nm, 80000x; d) 100 nm, 120000 nm; e) 100 nm, 100000x; f) 100 nm, 120000x.

nucleating into the β phase. So, this peak is also an evidence of structural changes of NLCs. The same happens with the other formulations of NLCs + VD3 when the morphologic characteristics indicated instability (Figure S1).

3.3. Cytotoxicity — Cell viability assessment

In the present work, Caco-2 cells were used to study the cytotoxicity of the NLCs through the resazurin assay. Fig. 3 indicates a reduction on Caco-2 viability (>30 %) for some of the conditions tested. Tested formulations are considered non-toxic because the percentage of cell viability is kept above 70 % (Doktorovova et al., 2014). The IC$_{50}$ values for each formulation were also calculated (Fig. 3a), indicating the concentrations that decrease the cell viability to 50 %. It was observed that after 24 h of incubation only NLCs1 + VD3 reached the IC$_{50}$ in the range of concentrations tested. For longer incubations (48 h) the IC$_{50}$ values obtained were between 0.25 and 0.50 gmg/mL, for all the formulations. 0.25 mg/mL and 0.1 mg/mL appear as safe concentrations demonstrating a good biocompatibility *in vitro* when incubated with Caco2 cells up to 48 h.

Fig. 3b shows the cell viability for 0.1 and 0.25 mg/mL of NLCs with VD3. The cellular viability was higher than 70 % for both concentrations and different time-points. In general, these results mean that NLCs concentrations of 0.25 mg/mL or lower do not have an effect on the metabolic activity of Caco-2 cells and demonstrate a good
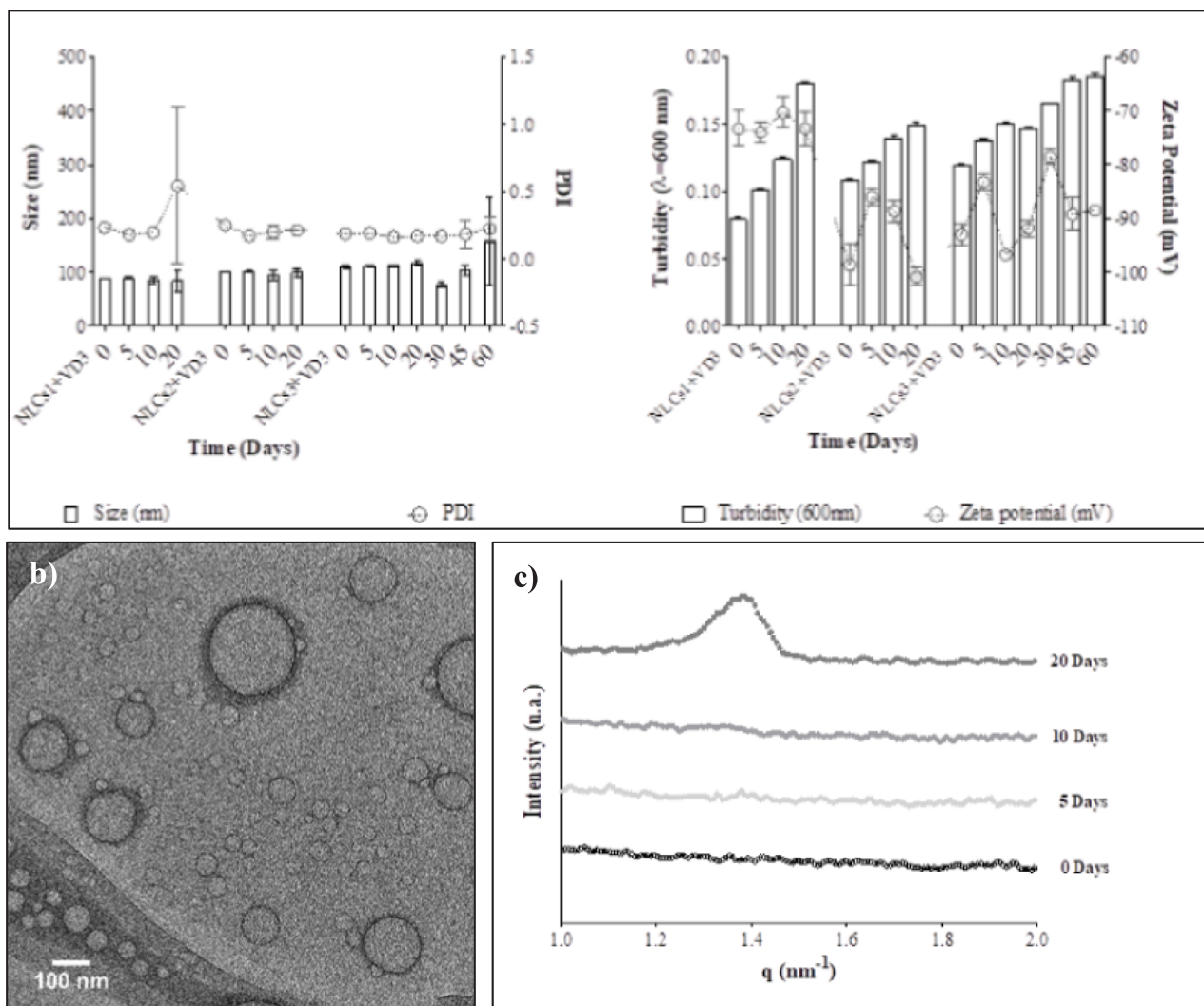
Fig. 2. a) Sizes, PDI, zeta potential and turbidity of all NLCs + VD3 formulations during storage at 4 °C; b) Transmission electron microscopy (TEM) images of NLCs1 + VD3 after 20 days of storage at 4 °C, Scale bar: 100 nm, 300000x; c) Small-angle X-ray scattering (SAXS) spectra of NLCs1 + VD3 1 during storage at 4 °C.
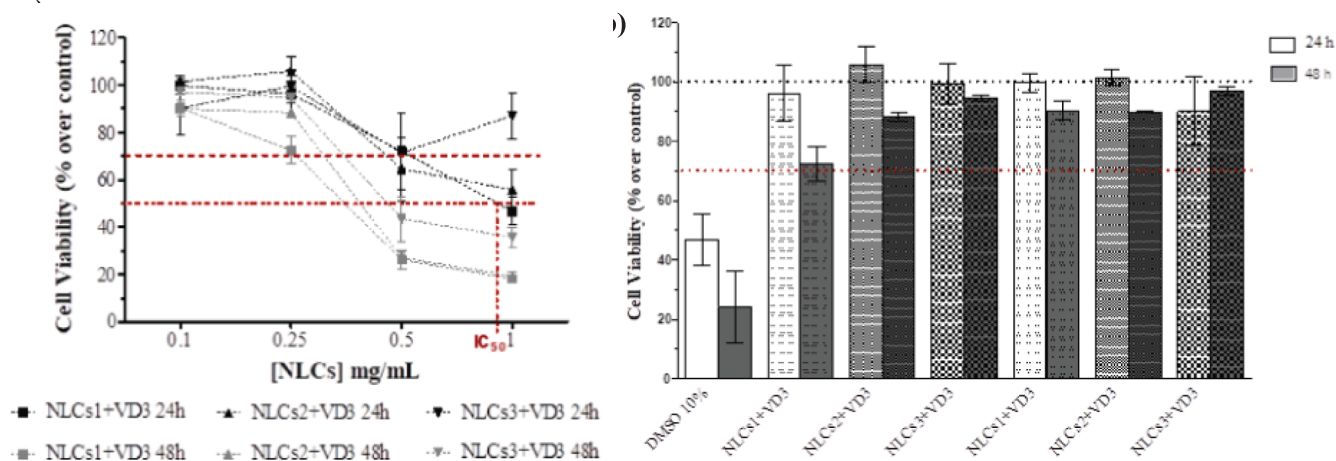

Fig. 3. Effect of NLCs + VD3 formulations on the cell viability of Caco-2 cells after incubation for 24 h and 48 h determined by resazurin assay.

biocompatibility *in vitro*. However, comparing the different NLCs between them, after 48 h of incubation the NLCs at 0.25 mg/mL presented a cellular viability increase in the following order: NLCs1 + VD3 < NLCs2 + VD3 < NLCs3 + VD3 ($p < 0.05$). This trend can be explained by the sizes of NLCs and/or the concentration of GM used in their development (Czjkowska-Kośnik et al., 2021). The cellular viability increases in the same order as sizes of NLCs, which can mean that the small sizes can affect their penetration into cells and induce more effect on the metabolic activity of Caco-2 cells. On the other hand, the ratio solid: liquid lipid was 20:80, 15:85 and 10:90 for NLCs1, 2 and 3, respectively. This means that the concentration of GM is different between them and can also explain the differences in cellular viability. This tendency was not observed in NLCs at 0.1 mg/mL ($p > 0.05$). The use of NLCs + VD3 in food or beverages turns the toxicological assessment mandatory (Lima et al., 2018). The results of this work show that using a concentration of 0.25 mg/mL or less of NLCs is not cytotoxic, which can be a good indication for its use in food or beverages (de Sousa et al., 2020).

3.4. Further analysis of NLCs + VD3

3.4.1. Extraction method assessment

For the extraction of VD3 from the NLCs, two extraction methods were tested: method 1 (Mtd 1) based on the work of Maurya & Aggarwal (2019) and method 2 (Mtd 2) built taking into account the works of Schoener, et al. (2019) and Tan, et al. (2019) (Maurya & Aggarwal, 2019; Schoener et al., 2019; Tan et al., 2019). The objective was to test which method would be more efficient to extract the VD3 from the initial NLCs and know the exact amount of VD3 encapsulated into each NLC. Both methods used high-performance liquid chromatography (HPLC) to quantify the vitamin. The HPLC has become popular in detecting vitamins like VD3 due to its rapid separation, high sensitivity, and accurate quantitation. The chromatographic conditions, such as analytical column, mobile phase composition and flow rate, were optimized to obtain the best peak shape, resolution, and retention time.

To calculate the concentration of VD3 extracted the maximal theoretical VD3 concentration encapsulated in the NLCs was considered. But, since the MCT used to produce the NLCs contains VD3, the vitamin concentration in the MCT was added to do these calculations. According to the supplier, the MCT contains a concentration of VD3 in the range of 2.50——2.75 %. So, assuming an average value of 2.625 % VD3, and considering the different ratios of solid:liquid lipids used for each formulation, the concentration (mg/mL) of VD3 was calculated for each NLCs (theoretical values), as can be seen in Table 1.

Initially, Mtd 1 was tested using DMSO and hexane to break up the particles and extract the VD3, respectively. However, this method provided VD3 concentration values lower than expected comparing to the theoretical (Table 1), suggesting that Mtd 1 was not efficient to extract the VD3 from the NLCs. The VD3 is almost insoluble in water and only sparingly soluble in DMSO explaining the low recovery observed

Table 1
Concentration values of VD3 obtained for each extraction method and the theoretical values.

[VD3]$_{initial}$ (mg/mL)	NLCs1 + VD3	NLCs2 + VD3	NLCs3 + VD3
Theoretical Values	0.210	0.223	0.236
Mtd 1	0.042 (±0.003) [a, A]	0.045 (±0.012) [a, A]	0.045 (±0.030) [a, A]
Mtd 2	0.273 (±0.020) [a, B]	0.285 (±0.022) [a, B]	0.277 (±0.005) [a, B]

Values are expressed as mean ± standard deviation.
Small letters are used to compare the different samples using the same extraction method (NLCs1 + VD3 *versus* NLCs2 + VD3 *versus* NLCs3 + VD3). The capital letters compare the Mtd1 and Mtd2 for the same sample. Different letters in same row/column indicate a statistically significant difference ($p < 0.05$).

(Almarri et al., 2017). Besides, NLCs + VD3 composition had a 99 % of aqueous phase, and therefore, the use of DMSO and hexane would not be the most appropriate solutions to solubilize VD3, explaining its incomplete extraction from the NLCs. VD3 is also unstable when exposed to ambient conditions resulting in degradation products like pre-vitamin D3, *trans*-vitamin D3, lumisterol D3, and hydroxyvitamin D3. Since these compounds have different retention times and UV absorptions (Temova & Roškar, 2016), was also tried to identify the degradation products by HPLC. However, none of the VD3-related compounds was detected suggesting that the degradation of VD3 does not explain the lower values obtained with Mtd 1.

On the other hand, Mtd 2 used hexane:ethanol (1:1, v/v) as extraction solution and mechanical disruption (vortex) and centrifugation to promote the break-up of the particles. With this method, concentrations of VD3 closer to the theoretical values were obtained (Table 1). The good solubility of VD3 in ethanol can explain the results (Almarri et al., 2017). However, the concentrations obtained for each formulation were slightly higher than expected. The MCT used to form the NLCs has DL-α-tocopherol (vitamin E) as stabilizer (max. 1 %), having a maximum absorbance peak at a wavelength at 292 nm and also a good affinity to ethanol. For this reason, was performed a spectrum analysis (200–400 nm, split 5 nm) during each run of the samples in the HPLC. The chromatograms of the samples were compared with a control run with Vitamin E ((±)-α-tocopherol, Sigma-Aldrich (Merck Group KGaA), Germany), and it was possible to identify a peak corresponding to vitamin E in all samples. Therefore, the presence of Vitamin E would account for this higher concentration of VD3.

3.4.2. In vitro digestion

The different formulations of NLCs + VD3 were evaluated through an *in vitro* gastrointestinal model to understand their fate under digestive conditions. The structural properties, the free fatty acids and the bio-accessibility of VD3 for each NLC + VD3 formulation were analysed at the end of the gastric and intestinal phases.

3.4.2.1. Structural analysis. The structural changes of NLCs + VD3 were evaluated by confocal fluorescence microscopy using Nile Red that stains lipids. Figure 4 shows the NLCs along the digestive system: gastric and intestinal phases. In the initial NLCs + VD3 formulations (before digestion), it was not possible to observe NLCs (results not shown) due to the resolution of the confocal microscope (0.2 – 0.5 μm) compared to the sizes of NLCs + VD3 (around 100 nm).

After the gastric phase, it was possible to see spherical red particles in all samples which can be explained by the increase of NLCs + VD3 size. This increase can be explained by flocculation, coalescence and/or Ostwald ripening promoted by the pH, salts and enzymes of the gastric phase. In the NLCs1 + VD3 formulation some aggregates were observed (Figure 4.a). This aggregation can be a result of flocculation because the individual oil droplets appear to have clustered together into large clumps but keeping their individual integrities. On the other hand, in NLCs2 + VD3 and NLCs3 + VD3 no aggregation is observed, so the size increase can be explained by coalescence (particles merge together to form a larger particle) and/or Ostwald ripening (molecular diffusion of oil molecules through the aqueous phase leads to the large particles grow and the small ones shrink) (McClements, 2013). The rhamnolipids have a pKa around 4–5 and when subjected to a pH lower than 5 acquired a neutral charge. Thus, it is possible that the electrical charge of the NLCs + VD3 changed from negative to neutral/positive during the gastric phase. As a consequence, the electrostatic repulsion decreased and attractive interactions (e.g., van der Waals) may have happened between the NLCs + VD3 leading to their fusion (Bai & McClements, 2016; Jahan et al., 2020). In NLCs1 + VD3 and NLCs2 + VD3 formulations some residues were observed (Figure 4.a2 and b2). These residues can be related with some GM loss from NLCs structure. During stability studies it was observed instability for these two formulations at
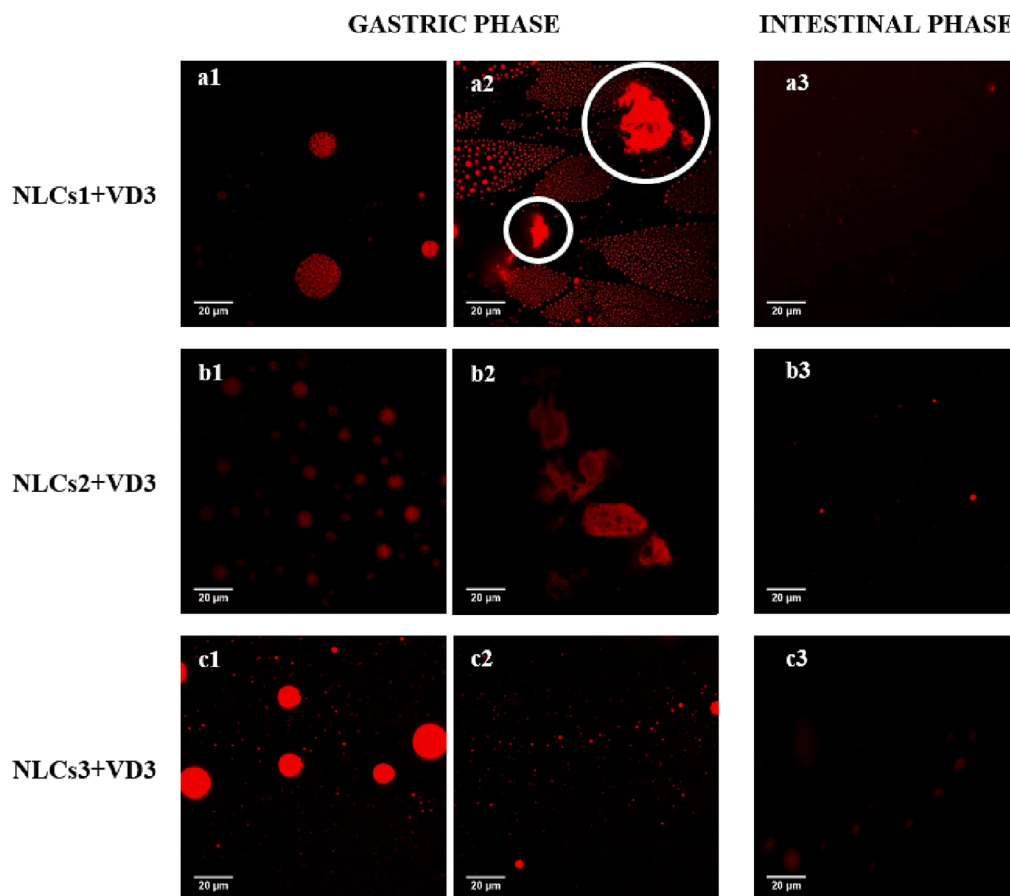
GASTRIC PHASE **INTESTINAL PHASE**

Fig. 4. Impact of gastric and intestinal phases on NLCs+VD3 monitored by confocal microscopy. Scale bar: 20 μm.

37 °C. The residues were not observed in NLC3s + VD3. Considering the liquid:solid ratio of each formulation, the NLCs3 + VD3 is the formulation with less solid lipid (GM). This way, the absence of residues can be related to this fact, which means that low GM concentration results in less or absence of residues under gastric phase conditions.

After the intestinal phase, the confocal images of all samples showed that most of the NLCs + VD3 disappear, and a low fraction of small particles was observed (Figure 4). This fact can be explained by the formation of mixed micelles as a consequence of lipid digestion (lipolysis) promoted by pancreatic enzymes and bile. The hydrolysis of triglycerides (a component of NLCs) produce anionic free fatty acids and neutral monoglycerides fluids that in the simulated intestinal fluid are incorporated into colloids called mixed micelles (Tan, Zhang, Muriel Mundo, et al., 2020; Tan, Zhang, Zhou, et al., 2020). In human gut, these colloids assemblies can act as carriers of fat-soluble molecules to the intestinal wall, where their absorption into the cells occurs (Euston, 2017).

So, despite the increase of their sizes and some GM loss from NLCs structure, these results show that the NLCs + VD3 have some resistance to the gastric phase conditions. However, under intestinal phase environment, all the NLCs are reduced to smaller sizes. This means degradation to be further incorporated into colloidal assemblies that can transport fat soluble molecules, such as vitamin D3, through the intestinal epithelium (intestinal absorption) increasing their bioaccessibility.

3.4.2.2. Bioaccessibility of VD3. The bioaccessibility of VD3 encapsulated within the three formulations of NLCs was measured at the end of the intestinal phase. The VD3 bioaccessibility values for NLCs1 + VD3, NLCs2 + VD3 and NLCs3 + VD3 were 65.80 %, 72.72 % and 51.57 %, respectively. It is also possible to observe the influence of GM:MCT ratio on the VD3 bioaccessibility. Ozturk, et al. (2015) studied the effect of

different oils (MCT, corn, fish, orange, and mineral oils) on VD3 bioaccessibility (Ozturk et al., 2015). They showed that the bioaccessibility of VD3 was highly dependent on the type of oil used to form the nano-emulsions. The MCT oil presented lower values of VD3 bioaccessibility although MCT was fully digested. Ozturk and co-workers explained that these results can be attributed to the micelles obtained after digestion. The corn and fish oils are formed by long-chain fatty acids which form mixed micelles with larger non-polar regions with the capacity to accommodate large lipophilic bioactive molecules. On the other hand, the MCT is constituted by medium-chain fatty acids and, as a consequence, it forms mixed micelles with smaller non-polar regions being more difficult to accommodate the lipophilic compounds inside. Schoener, et al. (2019) also studied the influence of different oils on VD3 bioaccessibility (Schoener et al., 2019). Beyond to the same conclusion of Ozturk and co-workers, Schoener and co-workers explained that the bioaccessibility differences between the oils can also be attributed to the rate and extent of lipolysis. Considering the GM:MCT ratio in each NLC, the bioaccessibility values obtained can be explained by the rate and extent of lipid digestion that can lead to different mixed micelles during the intestinal phase. Furthermore, mixed micelles have a maximum solubilization capacity. Its means that once the micelles are saturated, no more vitamin can be incorporated (Zhou et al., 2021). In addition to that, the VD3 is known to isomerize and/or degrade under various conditions like temperature, iodine, acidic conditions and oxidation. This way, the values lower than 100 % can be explained by the degradation of VD3 that is not incorporated within mixed micelles (Winuprasith et al., 2018).

3.4.2.3. Lipid digestion. The lipid digestion takes place during the intestinal phase. The lipase in the intestinal fluid absorbs at the oil surface of the lipid-based nanosystem hydrolysing triacylglycerols (TAG). In

general, each molecule of TAG generates two free fatty acids (FFAs) and one monoacylglycerol (MAG). At the same time, the lipolysis products are removed from the oil–water interface by bile salts forming mixed micelles where lipid soluble components can be incorporated and transported (Li & McClements, 2010; Verkempinck et al., 2018).

In the present work, the intestinal digestion of the NLCs + VD3 was monitored using a pH-stat method to evaluate lipid digestion (lipolysis). Fig. 5a shows the volume of NaOH needed to maintain the pH at 7.0 for each NLC during the intestinal phase. All the NLCs presented a rapid increase in the NaOH volume added during the first 8 – 10 min and then no more NaOH was added. This means that the lipid digestion and, consequently, the FFAs release occurred in the first minutes of the intestinal phase. Relatively to the total volume of NaOH added for each sample, the NaOH volume increase in the following order: NLCs3 + VD3 < NLCs1 + VD3 < NLCs2 + VD3. Taking into account the relation between the NaOH titrated and FFAs release, the percentage of FFAs had the same tendency. However, the final FFAs released by the end of the intestinal phase were: 43.89 %, 52.43 % and 34.91 % for NLCs1 + VD3, NLCs2 + VD3 and NLCs3 + VD3, respectively. Previous studies have shown that the FFAs generated during the lipid digested are not all deprotonated at neutral pH and a back titration to pH 9 is needed to detect any FFAs that were not ionized under neutral conditions (Tan, Li, Zhou, Liu, et al., 2020; Tan, Zhang, Zhou, et al., 2020). This way, it was done a second step where the pH was increased until 9 to detect the total percentage of FFAs released. In this case, higher values were reached being obtained 103.1 %, 88.79 % and 82.61 % for NLCs1 + VD3, NLCs2 + VD3 and NLCs3 + VD3, respectively (Fig. 5b). Indeed, for NLCs1 + VD3 was obtained values higher than 100 %. This fact can be explained by the production of more than two molecules of FFAs per TAG due to the alkaline hydrolysis of TAG molecules at high pH values. The

equation used to calculate the percentage of FFAs released Eq. (1) assumes the production of two FFAs and one MAG molecule per TAG. However, under alkaline pH the MAG molecules can also break down and form FFAs and glycerol (Tan, Li, Zhou, Liu, et al., 2020; Tan, Zhang, Muriel Mundo, et al., 2020; Tan, Zhang, Zhou, et al., 2020).

Considering the total of FFAs released after the intestinal phase (pH 7) and after the back titration (pH 9) was calculated a correction factor (CF):(Tan, Zhang, Zhou, et al., 2020)

$$CF = \frac{Final\ FFAs\ (pH\ 9)}{Final\ FFAs\ (pH\ 7)} \qquad (3)$$

Using the measured NaOH volumes during the intestinal phase and the CF, was calculated the corrected FFAs released (%) during the lipid digestion.

Fig. 5c shows the corrected FFAs values obtained for each NLCs formulation. The results showed an almost complete lipid digestion for NLCs1 + VD3 and NLCs2 + VD3. The differences observed between NLCs1 + VD3 and NLCs2 + VD3 with NLCs3 + VD3 can be explained by the sizes of the particles. As already referred before, the sizes increased in the following order: NLCs1 + VD3 < NLCs2 + VD3 < NLCs3 + VD3. However, the FFAs released was higher for the NLCs with the smaller sizes. This can be explained by the bigger surface area exhibited by the smaller NLCs which provides more space for the lipase molecules to bind (Li & McClements, 2010).

It was observed a burst release between the first 8 and 10 min (depending on NLCs + VD3 formulation) and then the FFAs released maintained constant until the end of the intestinal phase. This means that the total lipid digestion happened in the first 8 or 10 min of the intestinal phase for all NLCs + VD3 studied. The confocal images prove these results showed in Figure 4, where it is possible to see that after the
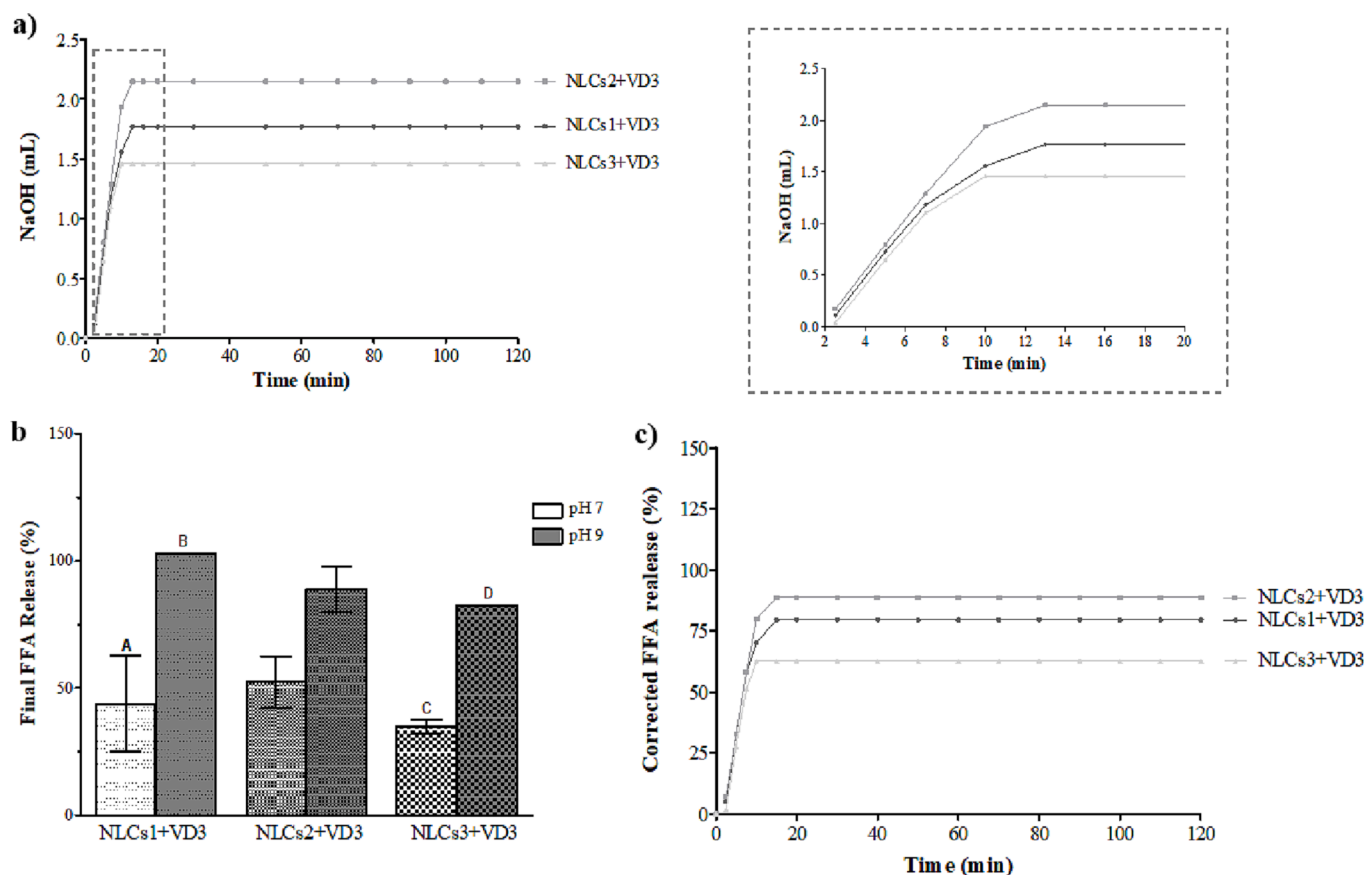

Fig. 5. Free fatty acid (FFA) assessment during the intestinal digestion of NLCs 1, 2 and 3 containing VD3 encapsulated: a) Volume of NaOH (0.05 N) required to maintain pH 7.0 during the intestinal phase; b) Final FFA released considering titration at pH 7.0 or pH 9.0; c) corrected FFA profile during the intestinal phase. For Final FFA released, different capital letters (A, B, C, and D) were used to designate a significant difference between samples at pH 7.0 and pH 9.0.

intestinal phase most of the NLCs + VD3 disappear, and a low fraction of small particles was observed. Furthermore, as observed by bio-accessibility results, the lipid phase composition (GM:MCT ratio) also had an influence on the rate and extent of lipid digestion.

4. Conclusions

VD3 was successfully encapsulated into the NLCs and the cytotoxicity assessment revealed that concentrations equal or lower than 0.25 mg/mL do not influence the metabolic activity of Caco-2 cells and demonstrate good biocompatibility *in vitro* being good evidence for its use in food or beverages. Regarding the *in vitro* digestion results, the VD3 bioaccessibility was influenced by the ratio of GM:MCT used. The NLCs3 + VD3 had more MCT than the others NLCs and obtained the lowest values of bioaccessibility. However, for this formulation was not observed residues after gastric digestion which can demonstrate a better stability under these conditions when compared with NLCs2 + VD3 and NLCs1 + VD3. At the end of the work, it was also evaluated lipid digestion during the intestinal phase and the lipid digestion of NLCs + VD3 was influenced by the nanosytem size and their composition.

CRediT authorship contribution statement

Maria A. Azevedo: Conceptualization, Investigation, Writing – original draft. **Miguel A. Cerqueira:** Conceptualization, Writing – review & editing, Supervision. **Catarina Gonçalves:** Methodology, Writing – review & editing. **Isabel R. Amado:** Methodology, Writing – review & editing. **José A. Teixeira:** Supervision. **Lorenzo Pastrana:** Supervision.

Declaration of Competing Interest

The authors declare that they have no known competing financial interests or personal relationships that could have appeared to influence the work reported in this paper.

Data availability

The data that has been used is confidential.

Appendix A. Supplementary data

Supplementary data to this article can be found online at https://doi.org/10.1016/j.foodchem.2023.136654.

References

Afonso, B. S., Azevedo, A. G., Gonçalves, C., Amado, I. R., Ferreira, E. C., Pastrana, L. M., & Cerqueira, M. A. (2020). Bio-based nanoparticles as a carrier of β-carotene: Production, characterisation and in vitro gastrointestinal digestion. *Molecules, 25* (19), 4497. https://doi.org/10.3390/molecules25194497

Almarri, F., Haq, N., Alanazi, F. K., Mohsin, K., Alsarra, I. A., Aleanizy, F. S., & Shakeel, F. (2017). Solubility and thermodynamic function of vitamin D3 in different mono solvents. *Journal of Molecular Liquids, 229*(March), 477–481. https://doi.org/10.1016/j.molliq.2016.12.105

Azevedo, M. A., Cerqueira, M. A., Fuciños, P., Silva, B. F. B., Teixeira, J. A., & Pastrana, L. (2021). Rhamnolipids-based nanostructured lipid carriers: Effect of lipid phase on physicochemical properties and stability. *Food Chemistry, 344*, Article 128670. https://doi.org/10.1016/j.foodchem.2020.128670

Babazadeh, A., Ghanbarzadeh, B., & Hamishehkar, H. (2017). Formulation of food grade nanostructured lipid carrier (NLC) for potential applications in medicinal-functional foods. *Journal of Drug Delivery Science and Technology, 39*, 50–58. https://doi.org/10.1016/j.jddst.2017.03.001

Bai, L., & McClements, D. J. (2016). Formation and stabilization of nanoemulsions using biosurfactants: Rhamnolipids. *Journal of Colloid and Interface Science, 479*, 71–79. https://doi.org/10.1016/j.jcis.2016.06.047

Bezerra, P. Q. M., de Matos, M. F. R., Ramos, I. G., Magalhães-Guedes, K. T., Druzian, J. I., Costa, J. A. V., & Nunes, I. L. (2019). Innovative functional nanodispersion: Combination of carotenoid from Spirulina and yellow passion fruit albedo. *Food Chemistry, 285*, 397–405. https://doi.org/10.1016/j.foodchem.2019.01.181

Brodkorb, A., Egger, L., Alminger, M., Alvito, P., Assunção, R., Ballance, S., … Recio, I. (2019). INFOGEST static in vitro simulation of gastrointestinal food digestion. *Nature Protocols, 14*(4), 991–1014. https://doi.org/10.1038/s41596-018-0119-1

Bruno de Sousa Sabino, L., Leônia da Costa Gonzaga, M., de Siqueira Oliveira, L., Souza Gomes Duarte, A., Alexandre e Silva, L. M., Sousa de Brito, E., Wilane de Figueiredo, R., Morais Ribeiro da Silva, L., & Machado de Sousa, P. H. (2020). Polysaccharides from acerola, cashew apple, pineapple, mango and passion fruit co-products: Structure, cytotoxicity and gastroprotective effects. *Bioactive Carbohydrates and Dietary Fibre, 24*, Article 100228. https://doi.org/10.1016/j.bcdf.2020.100228

Czajkowska-Kośnik, A., Szymańska, E., Czarnomysy, R., Jacyna, J., Markuszewski, M., Basa, A., & Winnicka, K. (2021). Nanostructured lipid carriers engineered as topical delivery of etodolac: Optimization and cytotoxicity studies. *Materials, 14*(3), 596. https://doi.org/10.3390/ma14030596

Doktorovova, S., Souto, E. B., & Silva, A. M. (2014). Nanotoxicology applied to solid lipid nanoparticles and nanostructured lipid carriers – A systematic review of in vitro data. *European Journal of Pharmaceutics and Biopharmaceutics, 87*(1), 1–18. https://doi.org/10.1016/j.ejpb.2014.02.005

Euston, S. R. (2017). Molecular simulation of biosurfactants with relevance to food systems. *Current Opinion in Colloid & Interface Science, 28*, 110–119. https://doi.org/10.1016/j.cocis.2017.04.002

Gonnet, M., Lethuaut, L., & Boury, F. (2010). New trends in encapsulation of liposoluble vitamins. *Journal of Controlled Release, 146*(3), 276–290. https://doi.org/10.1016/j.jconrel.2010.01.037

Grant, W. B., Al Anouti, F., & Moukayed, M. (2020). Targeted 25-hydroxyvitamin D concentration measurements and vitamin D3 supplementation can have important patient and public health benefits. *European Journal of Clinical Nutrition, 74*(3), 366–376. https://doi.org/10.1038/s41430-020-0564-0

Gupta, R., Behera, C., Paudwal, G., Rawat, N., Baldi, A., & Gupta, P. N. (2019). Recent Advances in Formulation Strategies for Efficient Delivery of Vitamin D. *AAPS PharmSciTech, 20*(1), 11. https://doi.org/10.1208/s12249-018-1231-9

Hewison, M. (2012). An update on vitamin D and human immunity. *Clinical Endocrinology, 76*(3), 315–325. https://doi.org/10.1111/j.1365-2265.2011.04261.x

Holick, M. F. (2007). Vitamin D Deficiency. *New England Journal of Medicine, 357*(3), 266–281. https://doi.org/10.1056/NEJMra070553

Jahan, R., Bodratti, A. M., Tsianou, M., & Alexandridis, P. (2020). Biosurfactants, natural alternatives to synthetic surfactants: Physicochemical properties and applications. *Advances in Colloid and Interface Science, 275*, Article 102061. https://doi.org/10.1016/j.cis.2019.102061

Katouzian, I., & Jafari, S. M. (2016). Nano-encapsulation as a promising approach for targeted delivery and controlled release of vitamins. *Trends in Food Science and Technology, 53*, 34–48. https://doi.org/10.1016/j.tifs.2016.05.002

Li, Y., & McClements, D. J. (2010). New mathematical model for interpreting pH-stat digestion profiles: Impact of lipid droplet characteristics on in vitro digestibility. *Journal of Agricultural and Food Chemistry, 58*(13), 8085–8092. https://doi.org/10.1021/jf101325m

Lima, H. L. S., Gonçalves, C., Cerqueira, M.Â., do Nascimento, E. S., Gama, M. F., Rosa, M. F., Borges, M. de F., Pastrana, L. M., & Brígida, A. I. S. (2018). Bacterial cellulose nanofiber-based films incorporating gelatin hydrolysate from tilapia skin: production, characterization and cytotoxicity assessment. *Cellulose, 25*(10), 6011–6029. https://doi.org/10.1007/s10570-018-1983-0

Marques, A. M., Azevedo, M. A., Teixeira, J. A., Pastrana, L. M., Gonçalves, C., & Cerqueira, M. A. (2019). Engineered Nanostructures for Enrichment and Fortification of Foods. In G. Molina, Inamuddin, F. M. Pelissari, & A. M. Asiri (Eds.), *Food Applications of Nanotechnology* (First ed., pp. 60–96). CRC Press - Taylor & Francis Group. doi: 10.1201/9780429297038.

Maurya, V. K., & Aggarwal, M. (2019). A phase inversion based nanoemulsion fabrication process to encapsulate vitamin D3 for food applications. *Journal of Steroid Biochemistry and Molecular Biology, 190*, 88–98. https://doi.org/10.1016/j.jsbmb.2019.03.021

McClements, D. J. (2013). Edible lipid nanoparticles: Digestion, absorption, and potential toxicity. *Progress in Lipid Research, 52*(4), 409–423. https://doi.org/10.1016/j.plipres.2013.04.008

Ozturk, B., Argin, S., Ozilgen, M., & McClements, D. J. (2015). Nanoemulsion delivery systems for oil-soluble vitamins: Influence of carrier oil type on lipid digestion and

vitamin D3 bioaccessibility. *Food Chemistry, 187*, 499–506. https://doi.org/10.1016/j.foodchem.2015.04.065

Park, S. J., Garcia, CV., Shin, G. H., & Kim, J. T. (2017). Development of nanostructured lipid carriers for the encapsulation and controlled release of vitamin D3. *Food Chemistry, 225*, 213–219. https://doi.org/10.1016/j.foodchem.2017.01.015

Pludowski, P., Holick, M. F., Grant, W. B., Konstantynowicz, J., Mascarenhas, M. R., Haq, A., … Wimalawansa, S. J. (2018). Vitamin D supplementation guidelines. *The Journal of Steroid Biochemistry and Molecular Biology, 175*(20), 125–135. https://doi.org/10.1016/j.jsbmb.2017.01.021

Salvi, V. R., & Pawar, P. (2019). Nanostructured lipid carriers (NLC) system: A novel drug targeting carrier. *Journal of Drug Delivery Science and Technology, 51*, 255–267. https://doi.org/10.1016/j.jddst.2019.02.017

Schoener, A. L., Zhang, R., Lv, S., Weiss, J., & McClements, D. J. (2019). Fabrication of plant-based vitamin D 3 -fortified nanoemulsions: Influence of carrier oil type on vitamin bioaccessibility. *Food & Function, 10*(4), 1826–1835. https://doi.org/10.1039/C9FO00116F

Soleimanian, Y., Goli, S. A. H., Varshosaz, J., & Sahafi, S. M. (2018). Formulation and characterization of novel nanostructured lipid carriers made from beeswax, propolis wax and pomegranate seed oil. *Food Chemistry, 244*, 83–92. https://doi.org/10.1016/j.foodchem.2017.10.010

Tamjidi, F., Shahedi, M., Varshosaz, J., & Nasirpour, A. (2013). Nanostructured lipid carriers (NLC): A potential delivery system for bioactive food molecules. *Innovative Food Science & Emerging Technologies, 19*, 29–43. https://doi.org/10.1016/j.ifset.2013.03.002

Tan, Y., Li, R., Liu, C., Muriel Mundo, J., Zhou, H., Liu, J., & McClements, D. J. (2020). Chitosan reduces vitamin D bioaccessibility in food emulsions by binding to mixed micelles. *Food and Function, 11*(1), 187–199. https://doi.org/10.1039/c9fo02164g

Tan, Y., Li, R., Zhou, H., Liu, J., Muriel Mundo, J., Zhang, R., & McClements, D. J. (2020). Impact of calcium levels on lipid digestion and nutraceutical bioaccessibility in nanoemulsion delivery systems studied using standardized INFOGEST digestion protocol. *Food & Function, 11*(1), 174–186. https://doi.org/10.1039/C9FO01669D

Tan, Y., Liu, J., Zhou, H., Muriel Mundo, J., & McClements, D. J. (2019). Impact of an indigestible oil phase (mineral oil) on the bioaccessibility of vitamin D 3

encapsulated in whey protein-stabilized nanoemulsions. In *Food Research International* (Vol. 120, pp. 264–274). doi: 10.1016/j.foodres.2019.02.031.

Tan, Y., Zhang, Z., Muriel Mundo, J., & McClements, D. J. (2020). Factors impacting lipid digestion and nutraceutical bioaccessibility assessed by standardized gastrointestinal model (INFOGEST): Emulsifier type. *Food Research International, 137*, Article 109739. https://doi.org/10.1016/j.foodres.2020.109739

Tan, Y., Zhang, Z., Zhou, H., Xiao, H., & McClements, D. J. (2020). Factors impacting lipid digestion and ß-carotene bioaccessibility assessed by standardized gastrointestinal model (INFOGEST): Oil droplet concentration. *Food and Function, 11* (8), 7126–7137. https://doi.org/10.1039/d0fo01506g

Temova, Ž., & Roškar, R. (2016). Stability-Indicating HPLC–UV Method for Vitamin D 3 Determination in Solutions, Nutritional Supplements and Pharmaceuticals. *Journal of Chromatographic Science, 54*(7), 1180–1186. https://doi.org/10.1093/chromsci/bmw048

Tipchuwong, N., Chatraporn, C., Ngamchuachit, P., & Tansawat, R. (2017). Increasing retention of vitamin D 3 in vitamin D 3 fortified ice cream with milk protein emulsifier. *International Dairy Journal, 74*, 74–79. https://doi.org/10.1016/j.idairyj.2017.01.003

Uluata, S., McClements, D. J., & Decker, E. A. (2016). Riboflavin-induced oxidation in fish oil-in-water emulsions: Impact of particle size and optical transparency. *Food Chemistry, 213*, 457–461. https://doi.org/10.1016/j.foodchem.2016.06.103

Verkempinck, S. H. E., Salvia-Trujillo, L., Moens, L. G., Charleer, L., Van Loey, A. M., Hendrickx, M. E., & Grauwet, T. (2018). Emulsion stability during gastrointestinal conditions effects lipid digestion kinetics. *Food Chemistry*. https://doi.org/10.1016/j.foodchem.2017.11.001

Winuprasith, T., Khomein, P., Mitbumrung, W., Suphantharika, M., Nitithamyong, A., & McClements, D. J. (2018). Encapsulation of vitamin D3 in pickering emulsions stabilized by nanofibrillated mangosteen cellulose: Impact on in vitro digestion and bioaccessibility. *Food Hydrocolloids, 83*, 153–164. https://doi.org/10.1016/j.foodhyd.2018.04.047

Zhou, H., Liu, J., Dai, T., Muriel Mundo, J. L., Tan, Y., Bai, L., & McClements, D. J. (2021). The gastrointestinal fate of inorganic and organic nanoparticles in vitamin D-fortified plant-based milks. *Food Hydrocolloids, 112*, Article 106310. https://doi.org/10.1016/j.foodhyd.2020.106310